on the pusher-shell interior, is most likely a nonuniformity in pusher-ion density (N_i) indicative of breakup of the pusher shell during target irradiation.

In addition to the above observations, the STX images provide some information about STE transport in short-pulse, exploding-pusher, microsphere targets. The STX simulation of Fig. 3 includes neither STE transport inhibition[8] nor enhanced azimuthal transport of STE's in the target sheath.[9] The good agreement between the images of Figs. 2 and 3 indicate that under favorable experimental conditions (i.e., quasiuniform illumination—no hot spots) such STE transport mechanisms probably do not play an important role in this class of laser fusion experiments.

We wish to acknowledge the assistance of our Lawrence Livermore Laboratory colleagues H. G. Ahlstrom, D. T. Attwood, Y. L. Pan, G. Howe, D. Ciarlo, C. Dittmore, W. Herrman, G. Stone, and the Shiva laser crew. This work was performed under the auspices of the U. S. Department of Energy under Contract No. W-7405-ENG-48.

[1]J. F. Kephart, R. P. Godwin, and G. H. McCall, Appl. Phys. Lett. 25, 108 (1974); V. W. Slivinsky, H. N. Kornblum, and H. D. Shay, J. Appl. Phys. 46, 1973 (1975); B. H. Ripin, *et al.*, Phys. Rev. Lett. 34, 1313 (1975).

[2]High-resolution imaging of the STX emission was found to be beyond the capabilities of pinhole and grazing incidence reflection techniques because of the low flux levels and high energies involved.

[3]Zone-plate coded imaging is a two-step imaging technique. In the first step the x-ray source casts a shadowgraph through a Fresnel zone plate onto an appropriate film. Image reconstruction (step two) is achieved optically with methods similar to holographic reconstruction. For further details see N. M. Ceglio, *et al.*, J. Appl. Phys. 48, 1563 (1977), and 48, 1566 (1977), and Phys. Rev. Lett. 39, 20 (1977).

[4]A layer in this pack consists of a filter foil followed by three single-sided x-ray films—types *M*, *R*, and *FGP*. The foil material, thickness, and x-ray image energies for the various layers are as follows: layer 1, Be, 150 μm, 4–7 keV; layer 2, Al, 250 μm, 10–20 keV; layer 3, Al, 1250 μm, 17– 30 keV.

[5]The image data format for all the figures is as follows: In the two-dimensional (2D) contour maps each contour is a locus of constant x-ray emission intensity. The incremental intensity change is constant between successive contours. In the 2D plots the two opposing ten-laser beam clusters are incident on the target from top and bottom. In the 3D plots the beam clusters are incident from the left and right, respectively. "Left" on the 3D plots corresponds to "top" on the 2D plots.

[6]LASNEX is a 2D Lagrangian, magnetohydrodynamics code with multigroup electron transport. For further details see G. B. Zimmerman, Lawrence Livermore Laboratory Report No. UCRL-78411, 1973 (unpublished).

[7]In these short-pulse, large-ball experiments, peak target compressions occur well after the peak of the laser pulse.

[8]S. Braginskii, *Reviews of Plasma Physics* (Consultants Bureau, New York, 1965), Vol. 1, p. 205.

[9]J. R. Albritton *et al.*, Phys. Rev. Lett. 39, 1536 (1977).

Structural Stability of 495 Binary Compounds

Alex Zunger
Solar Energy Research Institute, Golden, Colorado 80401
(Received 18 June 1979)

With use of the characteristic turning-point radii of the first-principles nonlocal density-functional atomic pseudopotentials, a successful topological prediction of the crystal structures of 495 binary *AB* compounds of transition and simple elements is obtained.

There are about 500 stable, near-stoichiometric, ordered binary solids made of atoms belonging to the first five rows of the periodic table whose crystal structure has been determined experimentally. Most of these crystals appear in their most stable form in one of about twenty distinct spatial structures. In this Letter I show that a simple nonempirical quantum mechanical approach, based on the density-functional nonlocal pseudopotential concept, explains this distribution diagrammatically with striking success.

Even before the pioneering studies of Goldschmidt, Pauling, and others[1] it was known thermodynamically that the structure-dependent energy ΔE_s of most ordered solids is small compared to either the cohesive energy ΔE_0 or the heat of formation. Measured heat-of-transformation data[2] as well as quantum mechanical calculations of stable and hypothetical structures indicate that $\Delta E_s/\Delta E_0$ can be as small as 10^{-3}–10^{-4}. For the 50–60 nontransition-metal binary octet compounds, the problem of systematizing the five crystal structures (NaCl, CsCl, diamond, zincblende, and wurzite) has been solved through the use of optical dielectric[3] as well as spectroscopic[4] electronegavity concepts. These concepts[5] display periodic trends diagrammatically when transferable elemental coordinates are used. Can the diagrammatic Pauling-esque approaches be extended to include intermetallic transition metal (TM) compounds as well?

While contemporary quantum mechanical models emphasize the decisive role of d electrons in determining the cohesive properties of TM compounds (e.g., Ref. 6), semiclassical approaches[7,8] have concentrated on more general phenomenological "factors" in an attempt to rationalize crystal structures. These include metallurgical and chemical constructs such as the atomic size, local geometry, coordination number, electronegativity, average electron count, and orbital promotion energy factors, where a certain subset of these ("strong factors") are frequently used to explain the occurrence of certain classes of compounds (usually 20–50 compounds at a time). The coexistence of many crystal structures in overlapping regions of these parameters, however, limits this approach to groups exhibiting narrow ranges of chemical properties. Nevertheless, these semiclassical approaches provide valuable insight into the problem because they point to the underlying importance of establishing elementary system-invariant *energy scales* (e.g., electronegativity, promotion energy) as well as *length scales* (e.g., covalent, metallic, or ionic radii).

In this Letter I show that the recently developed[9] first-principles density-functional nonlocal atomic pseudopotentials can provide nonempirical *angular-dependent* internal energy and length scales. By using a dual coordinate system derived from these scales I am able to obtain a topological separation of the structures of binary compounds (including simple and TM atoms) with a surpirizing accuracy.

The resulting pseudopotentials as well as a recent variant of them[10] have been shown to have a very small energy dependence[9] and to yield in self-consistent electronic structure calculations remarkably precise results for orbital energies and charge densities for atoms,[9,10] molecules,[11] bulk semiconductors[12] (e.g. for silicon deviation of 0.06 eV/state between the pseudopotential band structure and the full all-electron band structure, over a 20-eV range), and transition metals[13] as well as cohesive properties of elemental simple[14] and transition-metal[13] solids. They differ from the empirical and semiempirical potentials used extensively in the literature (e.g., Cohen *et al.*[15] and Appelbaum and Hamann[15]) in the occurrence of "hard-core" l-dependent classical turning points $V_{ps}^{(l)}$ ($r_l^{(0)}=0$ reflecting the high-momentum-transfer components $q>2k_F$ of the electron-core scattering).

I define the elementary nonlocal coordinates of an atom from the self-consistently screened pseudopotential $V_{eff}^{(l)}(r_l)=0$, where $V_{eff}^{(l)}(r) = V_{ps}^{(l)}(r)+V_{Coul}(n(r))+V_{xc}(n(r))+l(l+1)/2r^2$. These radii differ from those of St. John and Bloch[4] which were derived empirically from the spectra of single-electron ions for nontransition elements alone. I find that r_l^{-1} scales linearly with the experimental multiplet-average atomic ionization energies E_l. As r_l^{-1} reflects the scattering power of a screened atomic core to electrons with angular momentum l, the relation $r_l^{-1} = aE_l+b$ establishes r_l^{-1} as an intrinsic angular-momentum-dependent energy scale (much like the Thomas-Gordy and Mulliken electronegativity scales, which are, however, isotropic).

I similarly find that r_l scales linearly with the average position of the radial nodes in the "true" valence orbital $\psi_{nl}^{v}(r)$,[16] suggesting that r_l can also form an intrinsic length scale. The dual coordinates $\{r_l^{-1}, r_l\}$ hence satisfy the semiclassical ideas underlying successful structural indices[4,7,8] as well as the dual electronegativity-size mismatch constructs of alloy heat of formation models.[17] Similar characteristics of the empirically derived spectroscopic radii were first suggested by Bloch[16] for the nontransition elements octet systems.

I use the definition of structural indices for an AB compound suggested previously,[4,18] $R_\pi^{AB} = |r_p^A - r_s^A| + |r_p^B - r_s^B|$ and $R_\sigma^{AB} = |(r_p^A + r_s^A) - (r_p^B + r_s^B)|$, to construct structure-separation diagrams for the most stable phase of 109 octet $A^N B^{8-N}$ [Fig. 1(a)] and 351 nonoctet $A^N B^{P-N}$, $3 \leq P \leq 6$ [Fig. 1(b)], binary compounds. I arbitrarily define structural domains by calculating the smallest number of straight lines in the R_σ^{AB}

$-R_\pi^{AB}$ plane which minimize the number of "violations" and enclose minimal areas [Figs. 1(a) and 1(b)]. I am unable to separate the closely related NiAs($B8_1$) – MnP($B31$) and the CsCl($B2$) – CuAu($L1_0$) pairs [Fig. 1(b)] which show extemely small heats of transformation (often 1 kcal-mole) for compounds appearing in both forms.[2] Also I find that the seventeen $B20$ (FeSi) compounds, the ten $B19$ (AuCd) compounds, and the eight $B27$ (FeB) compounds [omitted from Fig. 1(b) for clarity] overlap precisely with the $B8_1$, $B2$, and $B33$ domains, respectively. These pairs of crystal structures are crystallographically very closely interrelated[19] and often coexist in narrow regions of thermodynamic parameters.[2] Otherwise, the number of "violations" in the present structure prediction is less than 7%. A better resolution of the TM-TM compounds belonging to the $B19$-$B2$-$L1_0$ structures may require a specialized scale involving d electrons more directly.

The success of the nonlocal atomic coordinates r_l in predicting crystal structures is nontrivial: Using the Miedema[17] heat-of-formation coordinates $\Delta\Phi_{AB}{}^*$ and $\Delta n_{AB}{}^{*1/3}$ or combinations of electronegativity differences ΔX_{AB} and various metallic or ionic radii ΔR_{AB}, or the Mooser-Pearson coordinates,[7] I find a poor *overall* structural separation over the present data base. It therefore seems that the radii of the screened first-principles nonlocal DF pseudopotential provide the best structural coordinates to data for the *full* data base of binary crystal structures available.

From the nonoctet compounds, two groups of *systematic errors* can be identified: The six $B2$ compounds appearing in the present plots in the $B8_1$-$B31$-$B20$ domain (CoAl, CoBe, CoGa, FeAl, FeGa, and NiAl) tend to support local magnetic moments; magnetic moments are indeed known[7] to alter significantly periodic trends in ΔE_0. The seven $B33$ compounds appearing in the $B2$ domain (AgCa, HfPt, NiHf, NiLa, NiZr, PtLa, and RhLa) are all characterized as *inverted* (i.e., $a/c<1$) $B33$ structures, more akin to the cubic $B2$ lattice.[20] The remaining violations (the experimentally reported structure and the presently assigned domain are denoted, respectively) are TiB ($B1$,$B33$), InPb ($B8_1$,$B2$), PtB ($B8_1$,$B1$), RhBi ($B8_1$,$B2$), NaPb ($tI64$,$B2$-$B32$), OsSi ($B2$,$B8_1$-$B20$-$B31$), PdBe ($B2$,$B33$), CoPt ($L1_0$,$B8_1$), and TiAl ($L1_0$,$B8_1$).

Interestingly, the present structural separation scheme predicts unusual electronic properties even within given structural groups: Whereas almost all of the 150 known bcc-like $B2+L1_0$ nonoctet binary compounds, are metals, the CsAu and RbAu systems appearing as an isolated subgroup in Fig. 1(b) were shown[21] to be semiconductors!

The success of the present dual coordinates in separating the crystal structures of many TM-TM and TM–non-TM compounds presents a striking result: The fact that the d electrons enter the nonlocal coordinates r_l only indirectly (via screening) suggests that the *structural part* ΔE_s of the cohesive energies of compounds may be determined by s-p coordinates (which, in turn, are found to be approximately linearly dependent on the d coordinate). This points to the possibility that while the localized d electrons determine *central-cell effects* (such as octahedral and Jahn-Teller ligand-field stabilization,[7] chemical trends in Mössbauer nuclear isomer shifts), and the regularities in the structure-insensitive cohesive energy[17] ΔE_0, the longer-range s-p wave functions are responsible for the stabilization of a certain complex space-group arrangement over another. While the resonant tight-binding (TB) models[6] have explained the periodic trends in the *structure-insensitive* part ΔE_0 of both elemental and alloyed TM systems by considering changes in the rectangular distributions of the one-electron d energy levels alone, it may be that in binary AB compounds with large differences in the constituent d-band energies, $E_d(A)\neq E_b(B)$, the s-p contribution to the *structural energy* ΔE_s is indeed dominant. If ΔE_s is derived primarily from Brillouin-zone–induced changes in the gaps E_{BZ} and these gaps can be divided into two groups $E_{BZ}{}^d$ and $E_{BZ}{}^{sp}$ (nonexistent in rectangular d density of states models), then the dominant structural role of s-p electrons becomes evident if covalent hybridation leads to $E_{BZ}{}^d \ll E_{BZ}{}^{sp} < E_d(A) - E_d(B)$. $E_{BZ}{}^{sp}$ is then expected to scale with R_π much like the heteropolar gaps.[17] It is remarkable indeed, however, that these complex *weak interactions*, often masked in elaborate calculations by errors in the *strong Coulombic interactions*, can be regularized by transferable s-p coordinates.

A complete account of the present work will be presented elsewhere. A table of all orbital radii used here is available from the author on request.

I am grateful to J. C. Phillips for comments and discussions. I am indebted to W. Andreoni

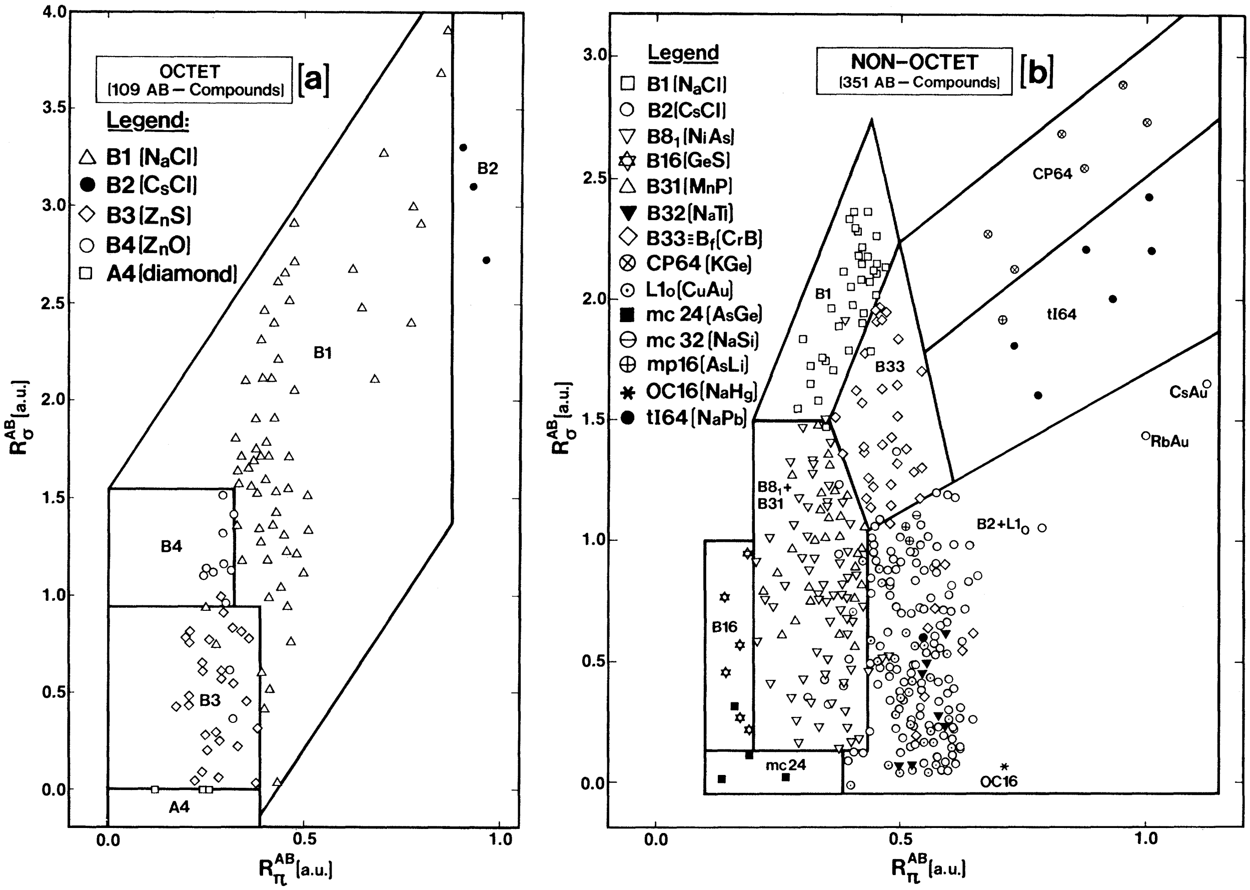

FIG. 1. Structural separation maps for *AB* compounds. The coordinates are $R_\pi{}^{AB} = |r_p{}^A - r_s{}^A| + |r_p{}^B - r_s{}^B|$ and $R_\sigma{}^{AB} = |(r_p{}^A + r_s{}^A) - (r_p{}^B + r_s{}^B)|$. The radii r_s and r_p mark the crossing points of the screened nonlocal atomic pseudopotentials. (a) Octet, (b) nonoctet.

and A. Baldereschi for indicating to me a numerical error in my previous Li r_p radius.

[1]L. Pauling, *The Nature of the Chemical Bond* (Cornell Univ. Press, Ithaca, N. Y., 1960).

[2]R. Hultgren, R. D. Desai, D. T. Hawkins, H. G. Gleiser, and K. K. Kelley, *Selected Values of the Thermodynamic Properties of Binary Alloys* (American Society for Metals, Metals Park, Ohio, 1973).

[3]J. C. Phillips and J. A. Van Vechten, Phys. Rev. B 2, 2147 (1970).

[4]J. St. John and A. N. Bloch, Phys. Rev. Lett. 33, 1095 (1974); E. S. Machlin, T. P. Chow, and J. C. Phillips, Phys. Rev. Lett. 38, 1292 (1977); G. Simons and A. N. Bloch, Phys. Rev. B 7, 2754 (1973).

[5]J. C. Phillips, Comments. Solid State Phys. 9, 11 (1978).

[6]J. Friedel, in *The Physics of Metals*, edited by J. M. Ziman (Cambridge Univ. Press, London, 1969), Chap. 8; D. G. Pettifor, Phys. Rev. Lett. 42, 846 (1979).

[7]W. B. Pearson, *The Crystal Chemistry and Physics of Metals and Alloys* (Wiley-Interscience, New York, 1972), pp. 51, 246.

[8]W. Hume-Rothery and G. V. Raynor, *The Structure of Metal Alloys* (The Institute of Metals, London, 1954); J. H. Westbrook, *Intermetallic Compounds* (R. E. Krieger Publishing Company, New York, 1977).

[9]A. Zunger and M. L. Cohen, Phys. Rev. B 18, 5449 (1978); A. Zunger and M. L. Cohen, Phys. Rev. Lett. 41, 53 (1978).

[10]A. Zunger, J. Vac. Sci. Technol 16, 1337 (1979).

[11]M. Schlüter, A. Zunger, G. P. Kerker, K. M. Ho, and M. L. Cohen, Phys. Rev. Lett. 42, 540 (1979).

[12]D. R. Hamann, unpublished; A. Zunger and M. L. Cohen, Phys. Rev. B 20, 4082 (1979).

[13]A. Zunger and M. L. Cohen, Phys. Rev. B 19, 568 (1979); A. Zunger, G. P. Kerker, and M. L. Cohen, Phys. Rev. B 20, 581 (1979).

[14]J. R. Chelikowsky, Phys. Rev. B (to be published).

[15]M. L. Cohen, M. Schlüter, J. R. Chelikowsky, and S. G. Louie, Phys. Rev. B 12, 5575 (1975); J. A. Appelbaum and D. R. Hamann, Phys. Rev. B 8, 1777 (1973).

[16]A. N. Bloch, unpublished; A. Zunger, unpublished.

[17]A. R. Miedema, J. Less Common. Met. 46, 67 (1976); J. R. Chelikowsky and J. C. Phillips, Phys. Rev. B 17, 2453 (1978).

[18]In the present application I use the absolute values $|r_p{}^A - r_s{}^A|$ as indicated in the text. This gives a somewhat better overall separation than the standard definition used in Ref. 9. Also, previous numerical errors in the Li and Na r_p values (Ref. 9) have been corrected ($r_p = 0.625$ and $r_p = 1.55$ a.u. for Li and Na, respectively). This improves on the separation of the eight Li and Na $B2$ compounds and reduces the separation of the $B32$ compounds.

[19]P. E. Blinger and K. Schübert, Z. Metall. 48, 126, 193 (1957).

[20]O. Schob and E. Parthé, Acta Crystallogr. 19, 214 (1965); D. Hohnke and E. Parthé, Acta Crystallogr. 20, 572 (1966).

[21]W. E. Spicer, Phys. Rev. 125, 1297 (1962); G. K. Wertheim and C. W. Bates, to be published.

Sublimation Rate of Cobalt near Its Curie Temperature

B. C. Sales, J. E. Turner, and M. B. Maple
Department of Physics and Institute for Pure and Applied Physical Sciences, University of California, San Diego, La Jolla, California 92093
(Received 21 May 1979)

Measurements are reported of the sublimation rate of cobalt in the vicinity of its Curie temperature ($T_C = 1400$ K) which show a relatively large change (~ 0.8 eV/atom) in the apparent activation energy for sublimation near T_C. The results can be accounted for in terms of a simple model that incorporates into the sublimation process the temperature dependence of the magnetic contribution to the binding energy of a cobalt surface atom.

The effects of magnetic and crystallographic phase transitions of metallic substrates on their oxidation kinetics have received increasing attention in recent years.[1-7] In particular, we reported that there is a relatively large change in the oxidation rate of nickel in the vicinity of its Curie temperature ($T_C = 631$ K).[5,6] The change in oxidation rate was manifested as a decrease of about 1 eV/atom in the apparent activation energy for oxidation as the nickel was heated above T_C. The typical oxide layers formed in this experiment were about 100 Å thick. For such thin oxide layers an important and possibly rate-limiting step in the oxidation process is the transfer of nickel ions through the nickel–nickel–oxide interface. The transfer[8] of nickel ions into nickel oxide is analogous to the sublimation of nickel atoms into vacuum and suggests that the sublimation rate of a ferromagnetic solid might also change upon passing through its Curie temperature. However, the ferromagnetic transition of nickel, and iron as well, occurs at too low a temperature to generate a measurable sublimation current. Fortunately, such an experiment is feasible for cobalt because of its relatively high Curie temperature ($T_C \approx 1400$ K). Measurements of the sublimation rate of cobalt in the vicinity of its Curie temperature are reported in this Letter.

A schematic diagram of the experimental arrangement is shown in Fig. 1. During the sublimation-rate measurements the pressure in the ultrahigh-vacuum chamber was kept below 3×10^{-9} Torr. A 0.0254-cm-thick cobalt foil was heated resistively by use of a high-current power supply. The cobalt atoms that sublimed from a small region near the center of the foil were deposited on a quartz-crystal thickness monitor held near room temperature. By monitoring of the change in the resonant frequency of the quartz crystal as a function of time, the rate of cobalt deposition and hence the sublimation rate could be determined. The temperature of the cobalt foil was measured and controlled to within ± 0.5 K using a Pt/Pt-13%Rh thermocouple spotwelded to the back of the foil. The Pt/Pt-13%Rh thermocouple was shielded from the harmful Co metal vapor by a 0.00254-cm-thick tantalum foil. In order to provide an additional check of the temperature, a resistance anomaly associated with the magnetic transition of cobalt was measured